Journal of New Technology and Materials (JNTM)
J. New Technol. Mater.
Vol. 11, N°01 (2021)24-32

OEB Univ. Publish. Co.

Design optimization of SAW temperature sensor based one port resonator using FEM simulation

N. Belkhelfa* and R. Serhane

Microelectronic and Nanotechnology Division, Centre de Développement des Technologies Avancées (CDTA). Cité 20 Août 1956, Baba Hassen, BP: 17, DZ-16303, Algiers, Algeria.

*Corresponding author, email: belkhelfa_n@yahoo.fr, nbelkhelfa@cdta.dz

Received date: Jan. 31, 2021 ; revised date: Apr. 03, 2021 ; accepted date: Apr. 04, 2021

Abstract

Surface acoustic wave (SAW) sensors fabricated on high-temperature piezoelectric substrates have attracted considerable attention due to their properties. Because it is important to model the SAW devices accurately, a simulation study of Rayleigh wave properties based on a stacked Al/AlN/Si (100) device was achieved, in this paper. Evolution curves of acoustic phase velocity, reflectivity and electromechanical coupling efficiency; for different aluminum (Al) electrode patterns and different piezoelectric aluminum nitride (AlN) layer thicknesses, were elaborated by 2D FEM COMSOL simulations. Added to that, the simulated acoustic mode shapes and the harmonic admittance of the device were represented. The best (AlN) layer thickness and electrode width were 1.5µm and 1µm respectively; they were deduced from the obtained SAW characteristics curves. After that, we used the deduced parameters for the conception of one port resonator temperature sensor working at a frequency of 1.166GHz. Using an elaborated theoretical temperature model coupled to FEM model, frequency shift induced by the SAW device temperature variation was evaluated from the return losses (S_{11}) parameter curves in a range of (-25°C to 200°C). The relative frequency change was about 0.17% and the sensor's sensitivity was evaluated at 8.53ppm/°C. Keywords: Surface Acoustic Wave; Phase velocity; Reflectivity; Return losses; Temperature coefficient of frequency; Sensitivity

1. Introduction

SAW devices are used in a multitude of products and applications in many fields as microelectromechanical systems (MEMS), telecommunications, chemical sensing and biotechnology [1-3]. The best characteristic of those devices is that they are wireless and passive. The sensor is remotely interrogated by an electromagnetic wave; this signal is transformed into an acoustic wave by means of transducers (an array of inter-digital electrodes) lying on the surface of a piezoelectric material. The acoustic wave propagating on this surface is transformed again into an electromagnetic wave and sent back to the interrogation unit by reflectors [1].

Precise determination of SAW parameters based on the device geometry and material characteristics is critical for designing a SAW device. By using appropriate design considerations, these devices become sensitive to external conditions including temperature, pressure, strain or chemical/biological mass loading [2]. SAW sensors are widely used for environment physical parameters measurement and accurate numerical methods as FEM analysis are used to optimize the design process [3]. Special attention is given to SAW devices geometrical parameters optimization as they affect SAW performances.

The current study is devoted to the conception of one-port SAW resonator able to detect temperature variation in the ambient environment. In the case of such sensors, temperature variation would result in a change in the SAW resonance frequency that generally shifts toward low values. Based on this variation, the extent of temperature change can be evaluated [4].

As SAW devices have the characteristic of being periodic, FEM modeling implemented by the commercial software COMSOL was used to model a unit cell SAW structure [5]. From the modal study, we obtain the eigenmodes shapes (mechanical displacement fields) and their corresponding symmetric and anti-symmetric frequencies. From the harmonic study, we deduce the SAW electrical response by means of the admittance curve and evaluate the resonance frequency variation with the device wavelength.

Using the eigenmodes resulting symmetric and anti-symmetric frequencies values, we study the evolution of acoustic phase velocity, the reflection coefficient and the electromechanical coupling factor of Rayleigh surface waves as function of (AlN) layer thickness. Those parameters characterize the Rayleigh SAW and they need

to be high [5,6]. The effect of electrode's height and width on SAW characteristics is also investigated.
At a later stage, the electrode width and piezoelectric layer thickness for which, we had the best reflectivity and coupling factor associated to a reasonable phase velocity are used in the design of one port SAW resonator intended to work as temperature sensor.
The temperature sensing is demonstrated by evaluating the (S_{11}) parameter of the sensor, which is characterized by the shift in the central frequency while temperature changes [7]. The performance of the SAW device in terms of sensitivity and the resonance frequency shift, for variation temperature levels between -25 °C to 200 °C is investigated. The decay of frequency when varying the temperature is also highlighted. The studied resonator has a center frequency f_0=1.166 GHz at room temperature; this frequency resulted from the chosen design parameters.

2. Simulated structure and Rayleigh mode shapes

In SAW devices, Rayleigh wave propagates over the surface of a piezo-substrate and its amplitude decreases exponentially with the depth of the substrate; so most of the energy is concentrated near the surface of the substrate [6]. In addition, the Rayleigh wave mechanical displacement field has two components: surface normal and surface parallel components. These characteristics allow modelling the SAW resonator device in two dimensions and with only three wavelengths depth of the substrate [6].
The infinite number of IDT fingers is modelled using periodic boundary conditions at the lateral extremities of the studied structure; the displacement and electric potential at both left and right periodic boundaries are made equal. The boundary conditions impose also the acoustic displacements and stresses to be continuous at the AlN-Silicon interface and both top and bottom sides of the structure to be stress free surfaces [6, 8].
A schematic of the layered structure is represented in Fig. 1.b; it consists of a Silicon (100) monocrystalline anisotropic substrate, (AlN) piezoelectric film and IDTs (Al electrodes). "h_{AlN}" is the thickness of (AlN) film, "λ" is the wavelength of the SAW, "a" the length of electrodes and "b" the pitch (spacing between electrodes), "*pml*" is a perfectly matched silicon layer. It is an absorbent layer used to avoid edge effects at the free ends of the structure; it forces the waves to damp by travelling a given distance inside it.

The wavelength is determined from geometry by:

$$\lambda = 2\times(a+b), \tag{1}$$

This wavelength is related to the central frequency of the SAW device f_0 by [1]:

$$f_0 = V_R / \lambda, \tag{2}$$

Where, V_R is velocity of Rayleigh wave.

The relation between stress T, strain S, electric field E and electric displacement D of piezoelectric materials is given by [1, 6]:

$$T_{ij} = c^E_{ijkl} S_{kl} - e_{kij} E_k \tag{3}$$

$$D_j = e_{jkl} S_{kl} - \varepsilon^S_{jk} E_k \tag{4}$$

e_{kij} is piezoelectric constant matrix, E_k is electric field vector, c_{ijkl} is elasticity matrix, S_{kl} is strain tensor, ε_{jk} is dielectric permittivity matrix.
FEM simulations (modal and harmonic analysis) are performed to evaluate the propagation of eigenmodes with and without metal electrodes. Those electrodes are electrical shorted in the modal study and polarized in the harmonic one (drive voltage is applied). The eigenmodes that are issued from the modal study represent the stopband edges of the surface waves (Rayleigh waves), i.e. in this stopband resulting from the coupling of modes, the waves propagation into the medium is minimum [8]. The width of the stopband depends on the magnitude of the reflection coefficient, according to (5) and (6) [3, 5, 6].
Anti-symmetric mode frequency

$$f_{m+} = (1+rp/\pi) f_0 \tag{5}$$

Symmetric mode frequency

$$f_{m-} = (1-rp/\pi) f_0 \tag{6}$$

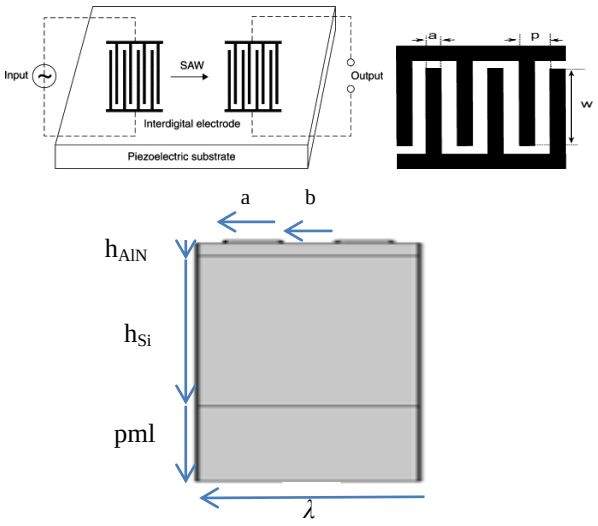

Figure 1. a) Schematic of SAW device and IDTs
b) Geometry of the unit cell used in the simulation.

3. Implemented model

Investigations on the structure of Fig.1 were done. Evaluation of the key design parameters as phase velocity v, reflectivity r and the coupling factor k^2 was accomplished. The purpose is to design a SAW device with good performances and CMOS (Complementary Metal Oxide semiconductor) compatible to benefit from

the opportunity of monolithic integration available in this process.

The equations used in the implemented model are [3, 5, 6]:

$$v = (f_{m+} + f_{m-}) \times p, \quad (7)$$

$$r = \pi \times (f_{m+} - f_{m-}) / (f_{m+} + f_{m-}), \quad 8)$$

$$k^2 = 2 \times (v_0 - v_m) / v_0, \quad (9)$$

v_0 is velocity of free (open) (AlN) surface, v_m velocity of metallized (shorted) AlN surface, p periodicity of the structure given by: $p = \lambda/2$.

4. Results and discussion

In the following, we study the effect of (AlN) film thickness on the SAW characteristics to understand the basic physical behavior.

First, a set of simulations on the structure of Fig.1, were conducted for varying electrode widths in the case of metallized (500 nm electrode height) and slightly metallized (1nm electrode height as free surface approximation) structure. Simulated electrode widths are 1µm, 2µm, 3 µm and 5µm which correspond to 4 µm, 8 µm, 12 µm, and 20 µm wavelengths respectively. The purpose is to determine the optimal value of electrode width and study the effect of electrode height "h_e" (IDT thicknesses of 1nm and 500 nm) on the SAW characteristics for different values of normalized (AlN) thickness (h_{AlN}/λ).

After that, simulations on a structure with an electrode width of 1µm (4 µm wavelength) and 500 nm height were achieved in order to find optimal values of (h_{AlN}) that give good velocity, reflectivity and coupling factor.

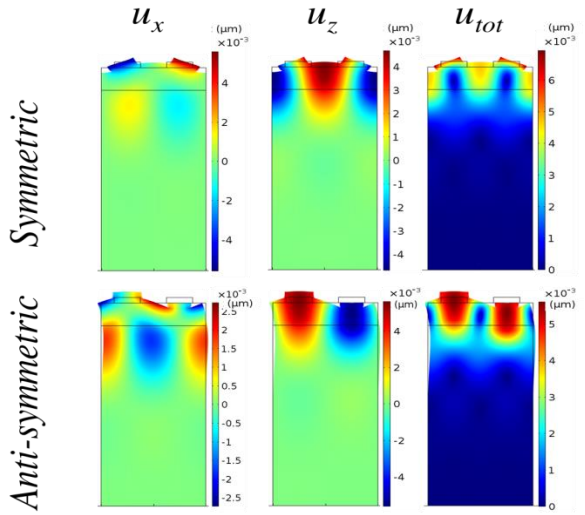

Figure 2. Mechanical displacement field components of symmetric and anti- symmetric modes

Fig.2 illustrates the shape of the total mechanical displacement field (associated to its u_x , u_z components); of the two first observed acoustic surface eigenmodes obtained with a structure of 1µm and 500nm IDT width and height respectively, and for (AlN) thickness h_{AlN}=1.5µm ($h_{AlN}/\lambda=0.125$). Those eigenmodes are the symmetric (f_m) and anti-symmetric ($f_{m'}$) displacement fields about the centerline obtained from eigenmode analysis available in the simulator, this analysis allows understanding of the elastic properties of the sample. The mode shapes of displacement profile (particle displacement) are helpful in recognizing the Rayleigh wave mode and determining precisely the acoustic wave propagation properties [5, 6]. The symmetric SAW mode gets its name from the fact that; the IDT vibrates symmetrically with respect to the mediator between two electrodes. It can be seen that the surface acoustic modes are confined to the top surface; between electrodes and the substrate-piezoelectric layer border.

The harmonic admittance, which characterizes the electrical behavior of the SAW device, is represented in Fig3, for every studied wavelength. The resonance frequencies, which are resonance frequency (f_R) and anti-resonance frequency (f_{AR}), coincide with the peaks in every admittance curve. With an electrode width of 1 µm, we obtain the biggest value of resonance frequency associated to the highest value of the admittance magnitude.

The resonance frequency that is defined as the eigenfrequency of the short-circuited electrodes is given by [3, 5]:

$$f_R = f_0 (1 + r / 2\pi), \quad (10)$$

This frequency is shifted from the center frequency (f_0) (ideal structure where resonance occurs at the center frequency) and depends on the reflectivity [2].

From the results of Fig.3, and according to (8), one expects to obtain the biggest value of reflectivity with 4 µm wavelength structure.

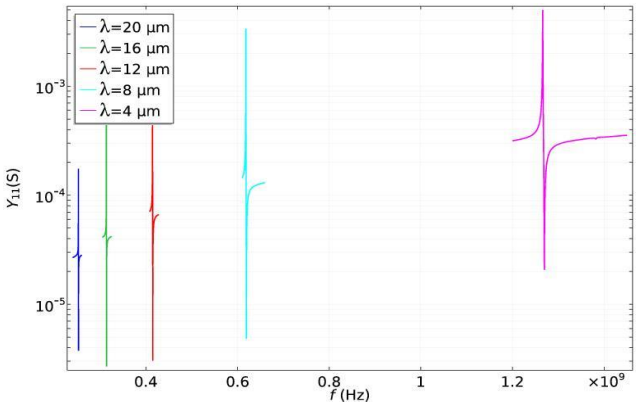

Figure 3. FEM admittance magnitude curves of the studied wavelengths

To obtain the values of velocity, reflectivity and coupling factor, we used the modal study resulting eigenmodes of the electrode widths of interest. The obtained stopband edges are represented in Fig.4.a and Fig.4.b, for slightly metallized (1nm electrode height) and metallized structure (500 nm). As the anti-symmetric SAW mode requires

more strain energy, it has a little higher frequency than the symmetric one [5].

In Fig.4a, the evolution of the stopband frequency edges for the parameter sweep of normalized (AlN) thickness (h_{AlN}/λ) is shown for different wavelengths; in the case of a free structure. The (f_{m+}) and (f_{m-}) obtained are almost identical because the reflection coefficient is quasi null (very thin layer of electrodes) which results in nearly identical frequencies (1) and (2).

In the case of a metallized structure (Fig.4.b), the highest values of frequencies (f_{m-} and f_{m+}) are obtained with 1µm electrode width (4µm wavelength). It can be seen that for all structures, the values of the obtained (f_{m+}) and (f_{m-}) still very close except for the 4µm wavelength structure, where the difference is around 0.2 GHz. This is explained by the results presented in Fig.7, where the reflectivity is the highest with 4µm wavelength.

This reflectivity has a direct effect on the symmetric and anti-symmetric frequencies values, according to (1) and (2). When the reflectivity is increased, the bandgap between symmetric and anti-symmetric modes is extended. On the opposite when the reflectivity is decreased, the frequencies degenerate into the central frequency (f_0) [8].

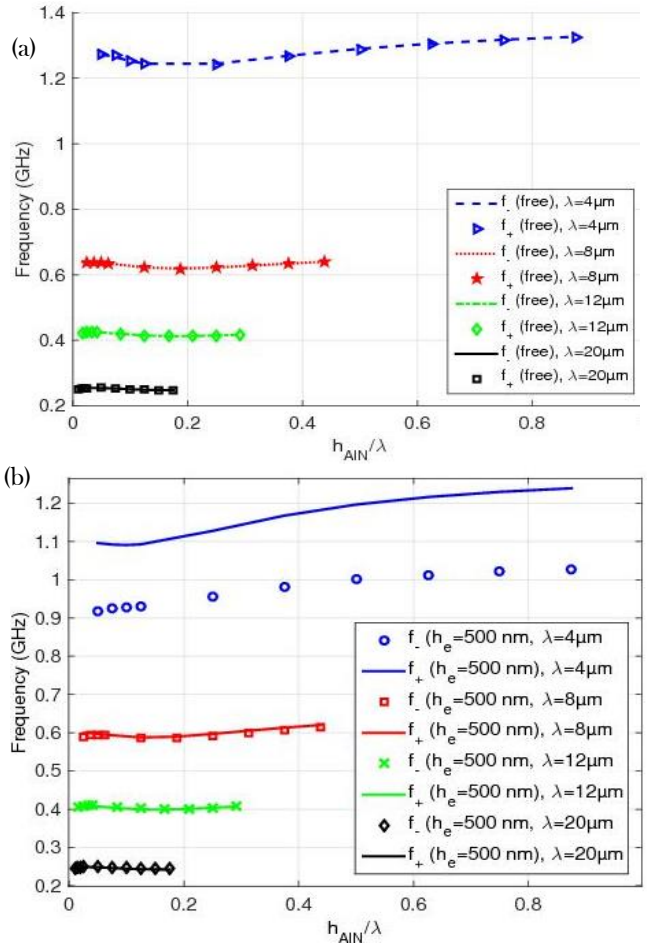

Figure 4. Frequency edges of the stopband for different electrode widths as function of normalized (AlN) thickness, a) free structure (h_e=0); b) 500 nm IDT height structure.

4.1 *Phase velocity*

In Fig.5a, the phase velocity variation curves obtained with an electrode height of 1nm are represented as function of (h_{AlN}/λ) for different wavelengths (λ); to obtain those curves (7) was used.

It can be seen that there is no difference in phase velocity when electrode widths change. This is due to the absence of mass loading effect (very thin electrodes) [6]. Many studies have proved that when metal surface increases (because of metallization ratio or electrode height increase), both phase velocity and resonance frequency decrease [9, 10]. In fact, SAWs are very sensitive to mass over their surface of propagation and the metal fabricated over the piezoelectric substrate exerts a mass load. This phenomenon induces unwanted effects in SAW devices response; like reduction of the highest SAW phase velocity that can be obtained with a structure of no metallic electrodes or neglected electrode height, which is the case in Fig.5a.

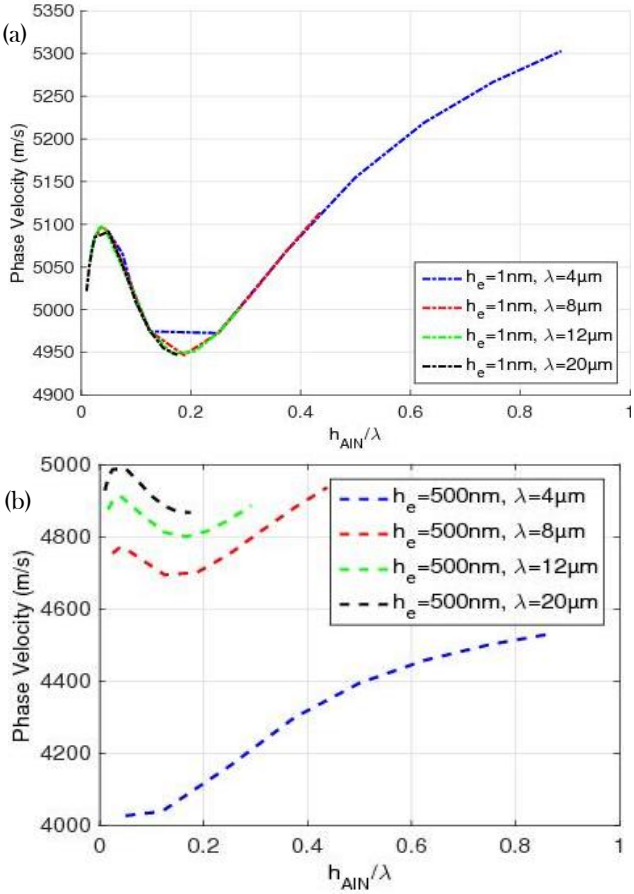

Figure 5. Phase velocities as function of normalized (AlN) thickness for different wavelengths, a) 1nm IDT height (h_e); b) 500 nm IDT height.

In Fig.5b, phase velocities obtained with an electrode height of 500 nm are represented for different wavelengths. Velocity increases with electrode width because SAW properties are influenced by the stopband width. The large width of the stopband obtained with 4µm

wavelength structure (Fig.4b) explains the obtained low velocity with the same structure.

In fact, the incident and reflected waves form a stopband by interfering constructively and destructively at (f_1) and (f_2) frequencies; the propagation into the medium is minimal at this stopband, which affects the velocity of the wave [8]. The obtained values of phase velocity are very close to those obtained in [5], where the velocities were in the range of 3000 (m/s) to 5000 (m/s) for (h_{AlN}) between 0.2 and 3 µm (the current study considered range).

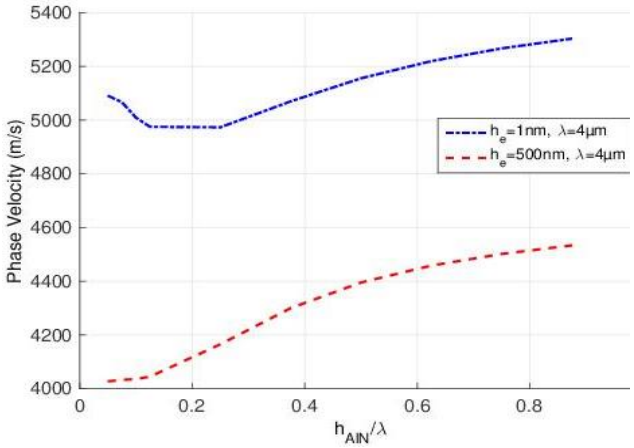

Figure 6. Phase velocity of 500 nm and 1nm IDT heights structures as function of normalized (AlN) thickness.

The phase velocity dispersion curve of Rayleigh mode in the Al/AlN/Silicon structure versus (h_{AlN}/λ) is represented in Fig.6 and this for an electrode width of 1µm and 1nm-500nm heights. We can see that phase velocity of the structure with 500 nm IDT height, is almost constant for low values of (AlN) thickness and that it increases from (AlN) thickness of 1 µm (h_{AlN}/λ=0.25); its value changes from 4000 (m/s) to 4600 (m/s). This is due to the large acoustic velocity of (AlN) (5760m/s) which dominates aluminum velocity when (AlN) thickness increases [6].

It also appears that velocity in a structure with 1nm electrode height is bigger than the velocity in 500 nm electrode height structure. In the case of 1 nm IDT height, velocity is around (5000 m/s) because it is overcome by the Rayleigh wave velocity of Silicon ($V_{R,Si(100)}$=5020m/s) [5,8], especially for low values of (h_{AlN}). Velocity of the 500 nm IDT is lower because the presence of electrodes creates an acoustic impedance and induces two effects: mechanical loading due to the mass of electrodes (already discussed); and electrical loading that is the shorting of electric field under the electrodes [10]. In effect added to the mass loading effect induced by IDTs, those later short circuit the parallel electric field associated with the SAW under them during wave propagation. The shorting of the electric field not only affects the SAW phase velocity but it also changes the resonance frequency of SAW resonators [10].

4.2 Reflection coefficient

To draw the reflectivity curves (8) was used. Actually, when varying (AlN) thickness, significant changes in the energy distribution of the symmetric and anti-symmetric modes occur, and those changes cause reflectivity to change [5]. The order of appearance of those modes determines the sign of reflectivity. Many design parameters affect the reflection; they are electrode material, the metallization ratio, the shape of electrodes and the electrode thickness [5].

Fig.7 illustrates the simulated reflectivity as function of (h_{AlN}/λ) for different electrode widths, in the case of 500 nm electrode height. The best value of reflectivity (around 0.3) is obtained for an electrode width of 1µm (λ=4µm). Those results fit well with the values obtained in [6], where the maximal value of reflectivity was 0.35 using Al electrode. The value of reflectivity depends on electrode's material density, which is 2.7g/cm^3 in the case of Al [6]. The high value of reflectivity obtained with 1µm electrode width structure explains the large bandgap obtained between (f_1) and (f_2) frequencies in the modal study of this structure.

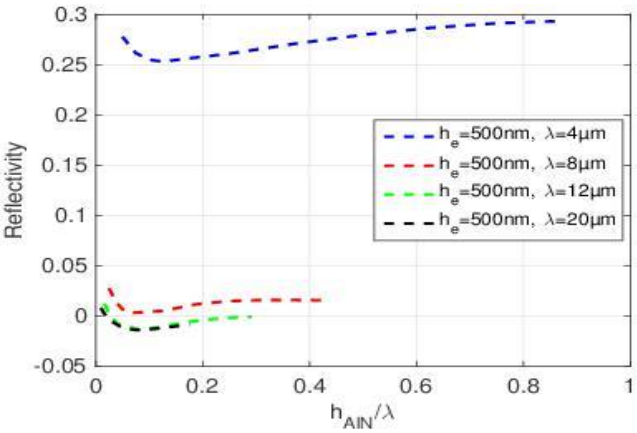

Figure 7. Reflectivity of a 500 nm IDT height structure as function of normalized (AlN) thickness for different wavelengths.

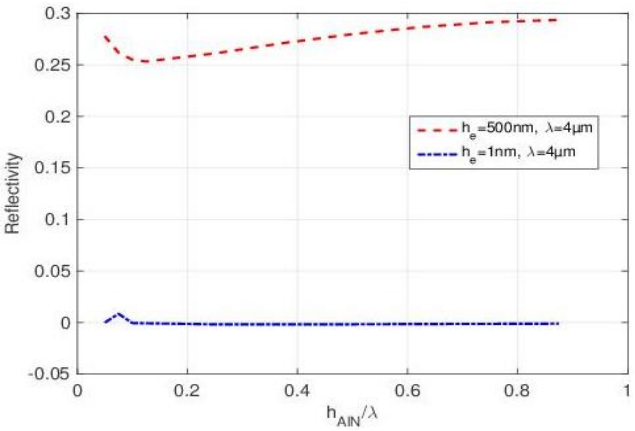

Figure 8. Reflectivity of 500 nm and 1nm electrode heights with 4µm wavelength structures, as function of normalized (AlN) thickness.

In Fig.8, the reflectivity of 1µm electrode width structure, in the case of 500 nm and 1 nm IDT heights, is represented. The reflectivity of the structure with 1 nm IDT is null (no IDTs approximation). For a 500 nm IDT height structure, in the case of the thin layer h_{AlN} = 0.2 µm (h_{AlN}/λ =0.05), the energy distribution is confined next to Al electrodes which results in a higher reflectivity. When the (AlN) thickness increases, the energy distribution is modified and causes reflectivity to decrease. This reflectivity increases significantly from (h_{AlN}) thickness of 1.5µm (h_{AlN}/λ =0.375). The reflectivity is no longer affected by the variation of AlN thickness from h_{AlN} around 3 µm (h_{AlN}/λ around 0.7); this is because of the constant energy distribution in the layer system [2, 6].

4.3 *Electromechanical coupling coefficient*

The electromechanical coupling factor curves versus (h_{AlN}/λ) are plotted in Fig.9; they were obtained using (9). "k^2" is a measure of the efficiency of a given piezoelectric in converting an applied electrical signal into mechanical energy associated with a surface acoustic wave [3].
It can be seen that the electrode width of 1µm exhibits the largest coupling coefficient (around 0.63%). The lowest pic of k^2 (around 0.4%) is obtained with a structure of 20µm wavelength (5µm width).

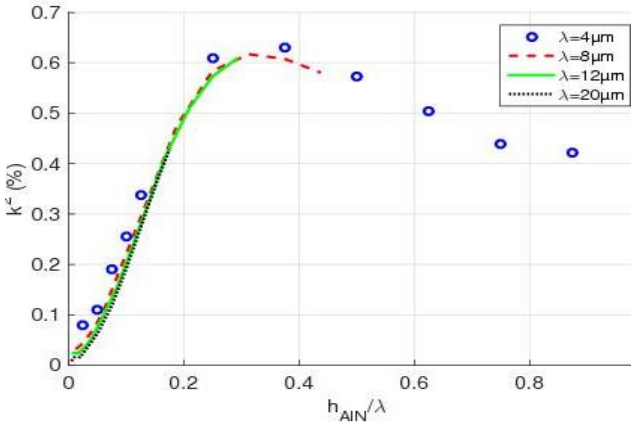

Figure 9. Coupling factor as function of normalized (AlN) thickness for different electrode widths.

For the structure with an electrode width of 1 µm and 500 nm height, the highest values of electromechanical coupling coefficient (0.50% to 0.63%) are obtained in the range of (h_{AlN}) from 1µm to 2.5µm (h_{AlN}/λ from 0.25 to 0.62). This is in good agreement with the experimental results obtained in [11] where the values of k^2 obtained were in the range of 0.5% to 0.6% for (h_{AlN}) from 1.2 µm to 2.4 µm.

4.4 Discussion

At the end of the analysis study, we conclude that an electrode width of 1µm gives better performances compared to the other widths, particularly the reflectivity and the coupling coefficient parameters. Although we did not obtain the best velocities with the 1µm electrode width, a compromise between selecting the wavelength that gives the best velocity or k^2 and reflectivity together is made.
Furthermore, the 1 µm electrode width gives the best admittance magnitude value. In the case of the structure with 1 µm electrode width and 500 nm height, the best piezoelectric layer thickness (h_{AlN}) is an interval ranging from 1µm to 2.5µm. With this (AlN) thickness, we have good reflectivity, and coupling factor combined.

The following study focuses on the design of one-port SAW temperature sensor using the geometrical parameters issued from the analysis of SAW properties and that gave reasonable performances. Our choice fell on 1 µm electrode width and 1.5 µm (AlN) layer thickness. The one port resonator was chosen instead of a two ports one because multiple research efforts proved that passive wireless SAW temperature sensors based on one-port resonators are excellent sensing elements with a high Q factor, they also proved that those resonators impose fewer demands on the coupling coefficient which allows the fabrication of small sensor elements [7].

5. Temperature sensor simulation

As we have seen in the previous study, SAW resonators are devices that present narrow signals in the frequency domain, with peaks at their resonance frequency and the corresponding anti-resonance frequency. Physical effects, like temperature variation shift the resonance frequency, which can be used to measure the temperature change. The thermal effects on the resonance frequency of SAW resonators are due to a change in the length of the substrate and the substrate material parameters (as density and elastic coefficients). Both of these phenomena affect the acoustic wave velocity, which causes a shift of the resonance frequency [12].

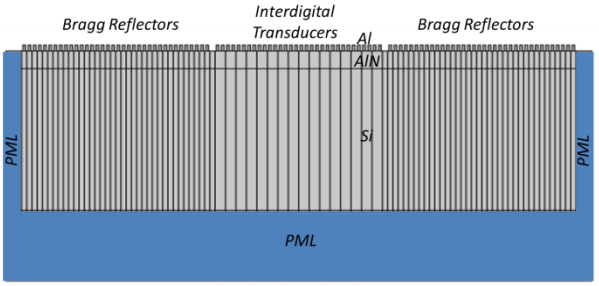

Figure 10. Schematic representation of one port resonator sensor.

The studied resonator is shown in Fig.10, it is formed of an (AlN) piezoelectric layer (which thickness h_{AlN} is 1.5 µm), deposited on a silicon substrate (100), the 16 pairs of aluminum inter-digital electrodes (IDTs) have a thickness

(h_e) of 500 nm, while the width (*a)* and spacing (*b)* are 1 µm each (λ=4µm).
An elaborated theoretical model for temperature change detection, coupled to FEM model was used in order to predict the sensor's behavior when subjected to temperature variation. The physical parameters affected by temperature variation were deduced from the literature [6, 13 and 14].

5.1 *TCF constant and sensitivity of the sensor*

The change of the resonance frequency due to temperature changes is described by the temperature coefficient of frequency (TCF).
(TCF) is one of the key parameters of a temperature sensor; it allows to evaluate the SAW's resonance frequency normalized shift (in ppm, part per million) for a variation of 1°C in temperature. In the case of SAW based temperature sensors, a large value of the (TCF) constant is very beneficial because it is itself the standard sensitivity ***S*** [ppm/°C] of the sensor.
The relation between TCF and the sensitivity is given by [15]:

$$S = \frac{1}{f_0}\frac{\partial f_0}{\partial T} = TCF\,, \tag{11}$$

This sensitivity can also be expressed without normalization by *s* [Hz/°C], according to (12):

$$s = \frac{\partial f_0}{\partial T}\,, \tag{12}$$

(TCF) is related to materials parameters as α_{11}, α_{22} and α_{33}, which represent the effective thermal expansion coefficients of the piezoelectric layer in the x, y and z directions respectively and α that is the thermal expansion of the substrate according to (13).

$$TCF = \frac{1}{2}\left[TCE - (\alpha_{11} + \alpha_{22} + \alpha_{33})\right] - \alpha \tag{13}$$

5.2 Parameters to be considered in simulation of a SAW temperature sensor

Actually, the change in the temperature of the surrounding environment and consequently sensor's temperature can cause two major effects, which are a change in the length of the propagation path and interdigital distance *d*, added to a change in material's density when it is deformed.
In order to construct a model of the SAW temperature sensor by Finite Element Method (FEM), we consider the variations of the physical parameters cited above and developed in the first order [14].

Interdigital distance

$$d = d(T_0)(1+\alpha.\Delta T)\,, \tag{14}$$

(AlN) thickness

$$h_{AlN} = h_{AlN}(T_0)(1+\alpha_{33}\Delta T)\,, \tag{15}$$

Density of the substrate

$$\rho(T) = \rho(T_0)\left[1-(\alpha_{11}+\alpha_{22}+\alpha_{33})\Delta T\right] \tag{16}$$

The elastic constants developed in the second order are given by:

$$c_{ij}(T) = c_{ij}(T_0)\left[1+TCE_{ij}\Delta T + TCE2_{ij}\Delta T^2)\right] \tag{17}$$

For (AlN) and (Si), the constants α_{11}, α_{22}, α_{33}, TCE_{ij}, $TCE2_{ij}$ and α are given in table (1) [13, 16].

Table 1: (AlN) and (Si) Physical parameters used in the model

		AlN	Si
elastic constants, c_{ij} [GPa]	c_{11} c_{12} c_{13} c_{33} c_{44} c_{66}	410.06 100.69 83.82 386.24 100.58 154.70	170
1st order TCE Tc_{ij} [10^{-6}/K]	Tc_{11} Tc_{12} Tc_{13} Tc_{33} Tc_{44} Tc_{66}	-10.65 -11.67 -11.22 -11.13 -10.82 -10.80	-63
2nd order TCE $T2c_{ij}$ [10^{-9}/K^2]	$T2c_{11}$ $T2c_{12}$ $T2c_{13}$ $T2c_{33}$ $T2c_{44}$ $T2c_{66}$	-20.61 -19.51 -19.88 -20.03 -20.36 -20.39	-52
piezoelectric stress coef., e_{ij} [C/m^2]	e_{15} e_{31} e_{33}	-0.48 -0.58 1.55	-
relative permittivity, ε_{ij}	ε_{11} ε_{33}	9 11	11.7 11.7
CTE, α_{ij} [10^{-6}/K]	α_{11} α_{33}	5.27 4.15	2.6 2.6
density, ρ [kg/m^3]		3260	2329

5.3 *Total mechanical displacement field*

The total mechanical displacement field at central frequency (f_0), o the studied detector is represented in Fig.11. It can be seen that the maximum of the mechanical displacement is localized near the electrodes, i.e. surface acoustic modes are confined to the top surface (higher magnitude near the electrodes caused by particle displacement close to electrodes-piezoelectric layer surface); which is a characteristic of Rayleigh wave.

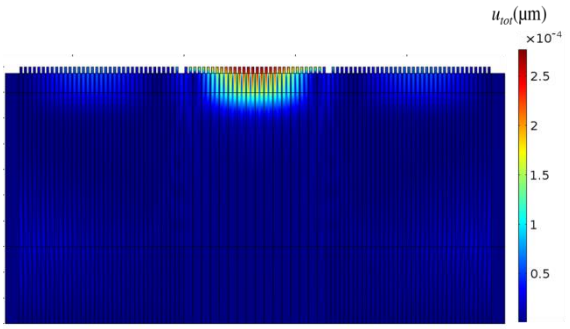

Figure 11. Mechanical displacement field at 1.166 GHz frequency.

5.4 *Return losses (S_{11} parameter)*

The reflection coefficient variation curves $S_{11}(f)$ for temperatures (T) ranging from -25°C to 200°C with a step of 25°C are shown in Fig.12. It is shown that, when temperature increases, (S_{11}) magnitude increases and its corresponding resonance frequency shifts toward low frequencies. The temperature behavior of (S_{11}) is attributed to the thermal expansion which would enlarge finger size and space, resulting is the increase of (λ). According to (2), (f_0) is inversely proportional to the wavelength (λ) and when (λ) increases (f_0) decreases. Obviously, the center frequency (f_0) has significantly reduced while temperature grew up to 200 °C. The SAW resonance frequency (f_0) shifted from 1166 MHz at 25 °C to 1164 MHz at 200 °C, providing a 0.17% relative frequency change.

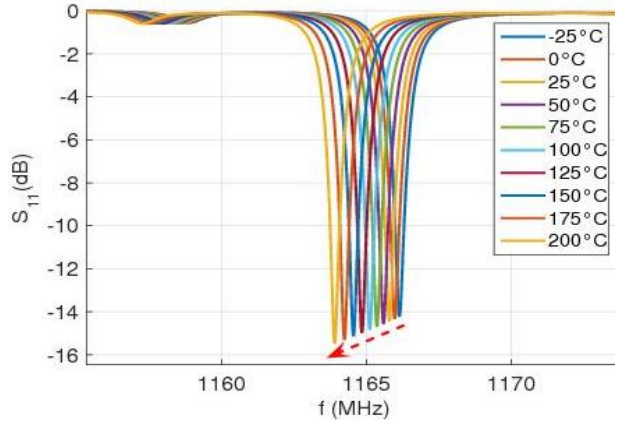

Figure 12. (S_{11}) Electrical response of the temperature sensor for different values of temperature

5.5 *Sensitivity of the sensor*

The relationship between frequency and temperature is plotted in Fig.13; a linear decrease as function of temperature is observed and the slope, which represents the sensitivity of the device (11,12), is given by a linear fit on the calculated values of the resonance frequency (f_0) shifts. The value of the sensor sensitivity (calculated from the slope of the obtained line) was s=9.94 kHz/°C, corresponding to S=8.53 ppm/°C (TCF of the structure).

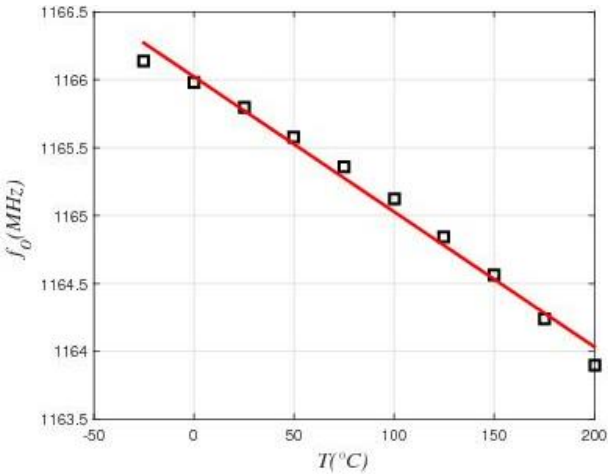

Figure 13. Resonance frequency shifts versus temperature.

6. Conclusion

When designing a layered SAW device, high velocity, coupling factor and reflectivity are all very important to obtain. Those parameters are dependent on the geometrical parameters and materials properties of SAW device. In this work, we used FEM simulation to analyze acoustic waves of SAW sensor based on Si substrate over which we have an (AlN) piezoelectric layer. The analyses were performed for different (Al) electrodes widths and AlN) thicknesses. The SAW characteristics were also investigated, in the case of free propagation approximation (1 nm electrode height) and the effects of IDTs have been highlighted. We found that an electrode width of 1µm gives good performances in terms of the coupling coefficient parameter (0.65%) and reflectivity (0.3), compared to the other widths. Based on those results, we chose λ=4µm and h_{AlN} =1.5 µm to design a one port SAW temperature sensor; the height of electrodes h_e was set to 500 nm.

To evaluate the frequency versus temperature variation of the studied structure, simulations on the SAW device were carried out from -25°C to 200°C using an elaborated theoretical temperature-sensing model coupled with the FEM model. We demonstrated different temperature behaviours of the SAW resonator by drawing the return losses (S_{11}) parameter characterized by the shift in the resonance frequency, when temperature changes.

The results showed that the variation of frequency with temperature exhibited good linear behavior. The center frequency of the resonator at 25 °C was 1.166 GHZ and it shifted to 1.164 GHz at 200°C, providing a relative decrease of 0.17%; while the sensitivity of the sensor was evaluated at S=8.53ppm/°C.

As an extension to this work, we intend to study other temperature sensors based on 2 µm and 3 µm electrode widths, for which we had acceptable performances. The aim is to reduce the center frequency of the sensor and evaluate its performance.

References

[1] Colin Campbell, Surface Acoustic Wave Devices and Their Signal Processing Applications, Academic Press, Kindle Edition, December 2012.

[2] V.Ionescu, Design and Analysis of a Rayleigh SAW resonator for gas detecting applications, Rom. J. Phys, 60, 3-4, 502-511.

[3] Ajay Tikka, Said Al-Sarawy, 2nd International Conference on Sensing Technology, SAW parameter extraction using finite element analysis, New Zeland, November 26-28, 2007, 393-398.

[4] Shuo Chen and Zheng You, Modeling and Experimental Analysis on the Temperature Response of AlN-Film Based SAWRs, Sensors, 16, (2016).

[5] Christian Kaletta, Christian Wenger, FEM simulation of Rayleigh waves for CMOS compatible SAW devices based on AlN/SiO2/Si (100), Ultrasonic, 54, (2014), 291-295.

[6] S.Maouhoub, Y.Aoura, A.Mir, FEM simulation of AlN thin layers on diamond substrates for high frequency SAW devices, Diamond and Relative Materials, 62, (2016), 7-13.

[7] Xuesong Ye, Qiong Wang, Lu Fang, Xuejun Wang, Bo Liang, IEEE Sensors Conference, Comparative Study of SAW Temperature Sensor Based on Different Piezoelectric Materials and Crystal Cuts for Passive Wireless Measurement, 1-4 November, USA, 2010, 583-585.

[8] J.G.Rodriguez, G.F. Iriarte, J.Pedros, Super-high-frequency SAW resonators on AlN/Diamond, IEEE Electron device letters, 33, 4, (2012), 495-497.

[9] Ashish Kumar Namdeo, Harshal B.Nemade, Comsol conference proceedings, FEM study of effect of metallic interdigital transducers on SAW velocity, India, 2011.

[10] Ashish Kumar Namdeo, Harshal B.Nemade, Simulations on effect of Electrical loading due to interdigital transducers in surfae acoustic wave resonator, Procedia Engineering, 64, (2013), 322-330.

[11] Lin Shu, Bin Peng, Chuan Li, The Characterization of surface Acoustic Wave Devices Based on AlN-Metal Structures, Sensors, 16, (2016), 526-536.

[12] G. Bu, D. Ciplys, M. Shur, L.J. Schowalter, S. Schujman and R.Gaska, Temperature Coefficient of SAW frequency in single crystal bulk AlN, Electronics Letters, 39, 9, (2003).

[13] Andrew B. Randles, Julius M. Tsai, Piotr Kropelnicki, and Hong Cai, Temperature Compensated AlN Based SAW, J. of Automation and Control Engineering, 2, 2, (2014), 191-194.

[14] Jan H. Kuypers, Chih-Ming Lin, Gabriele Vigevani and Albert P. Pisano, IEEE International Frequency Control Symposium (FCS), Intrinsic Temperature Compensation of Aluminum Nitride Lamb Wave Resonators for Multiple Frequency References, USA, May 2008, 19-21.

[15] Wenxiu Dong, Xue Ji, Jun Huang, Taofei Zhou, Tengkun Li, Yingmin Fan and Ke Xu, Sensitivity Enhanced Temperature Sensor-One port 2D surface phononic crystal resonator based on AlN/sapphire, Semicond. Sci. Technol, 34, (2019).

[16] Omar Elmazria and Thierry Aubert, Smart Sensors, Actuators and Mems Conference, Wireless SAW Sensor for high temperature applications -Material point of view, Prague, May 2011, 8066 806602-1